

# Roles of Residues Arg-61 and Gln-38 of Human DNA Polymerase $\eta$ in Bypass of Deoxyguanosine and 7,8-Dihydro-8-oxo-2'-deoxyguanosine\*

Received for publication, March 20, 2015, and in revised form, May 5, 2015. Published, JBC Papers in Press, May 6, 2015, DOI 10.1074/jbc.M115.653691

Yan Su, Amritraj Patra, Joel M. Harp, Martin Egli, and F. Peter Guengerich<sup>1</sup>

From the Department of Biochemistry and Center in Molecular Toxicology, Vanderbilt University School of Medicine, Nashville, Tennessee 37232-0146

**Background:** Arg-61 and Gln-38 of human DNA polymerase (hpol)  $\eta$  play important roles in the catalytic reaction.

**Results:** Mutations R61M or Q38A/R61A dramatically disrupt the activity of hpol  $\eta$ .

**Conclusion:** Polarized water molecules can mimic and partially compensate for the missing side chains of Arg-61 and Gln-38 in the Q38A/R61A mutant.

**Significance:** The positioning and positive charge of Arg-61 synergistically contribute to the activity of hpol  $\eta$ , with additional effects of Gln-38.

Like the other Y-family DNA polymerases, human DNA polymerase  $\eta$  (hpol  $\eta$ ) has relatively low fidelity and is able to tolerate damage during DNA synthesis, including 7,8-dihydro-8-oxo-2'-deoxyguanosine (8-oxoG), one of the most abundant DNA lesions in the genome. Crystal structures show that Arg-61 and Gln-38 are located near the active site and may play important roles in the fidelity and efficiency of hpol  $\eta$ . Site-directed mutagenesis was used to replace these side chains either alone or together, and the wild type or mutant proteins were purified and tested by replicating DNA past deoxyguanosine (G) or 8-oxoG. The catalytic activity of hpol  $\eta$  was dramatically disrupted by the R61M and Q38A/R61A mutations, as opposed to the R61A and Q38A single mutants. Crystal structures of hpol  $\eta$  mutant ternary complexes reveal that polarized water molecules can mimic and partially compensate for the missing side chains of Arg-61 and Gln-38 in the Q38A/R61A mutant. The combined data indicate that the positioning and positive charge of Arg-61 synergistically contribute to the nucleotidyl transfer reaction, with additional influence exerted by Gln-38. In addition, gel filtration chromatography separated multimeric and monomeric forms of wild type and mutant hpol  $\eta$ , indicating the possibility that hpol  $\eta$  forms multimers *in vivo*.

Y-family DNA polymerases are characterized by their low fidelity and ability to tolerate a wide range of lesions during DNA synthesis. Due to their relatively large active sites and loss of 3'-5' exonuclease domains compared with replicative DNA polymerases, they readily introduce mutations into the ge-

nome. These enzymes are able to insert dNTPs opposite and beyond DNA lesions, therefore rescuing blocked replication forks and releasing the arrested cell cycle (1–6).

Human DNA polymerase  $\eta$  (hpol  $\eta$ )<sup>2</sup> belongs to the DNA polymerase Y family (5). It plays a crucial role in bypassing cyclobutane pyrimidine dimers, which arise as a result of UV exposure. Defects in hpol  $\eta$  bypass of cyclobutane pyrimidine dimers in xeroderma pigmentosum variant patients results in increased rates of skin and internal cancers (7–9). hpol  $\eta$  contributes to replication past DNA lesions induced by platinum chemotherapeutic drugs, leading to escape of the arrested cell cycle and therefore proliferation of cancer cells (10–17). Besides translesion synthesis, there is evidence that hpol  $\eta$  is involved in homologous recombination by interaction with Rad51 and extension of the D-loop (18–20). hpol  $\eta$  also contributes to somatic hypermutation in B cells by introducing mutations in specific DNA stretches embedded within antigen-binding sites, thereby causing structural changes and potentially elevating the antigen-binding ability (21–27).

hpol  $\eta$  and its yeast homolog Rad30 also play roles in the bypass of 7,8-dihydro-8-oxoguanine (8-oxoG) (28–30), one of the most common DNA lesions introduced by oxidative stress. 8-oxoG is generated at a rate of >1000 molecules/cell/day and prefers the *syn* conformation, which facilitates formation of a Hoogsteen pair with dATP and introduces mutations into the genome (31–33). hpol  $\eta$  replicates past 8-oxoG mainly by inserting dCTP, scaffolding the dCTP:8-oxoG pair in the Watson-Crick geometry, although the dATP misincorporation rate is 280-fold higher in the bypass of 8-oxoG compared with unmodified G (30).

Crystal structures of the catalytic core of hpol  $\eta$  (amino acids 1–432) and its yeast homolog with unmodified or lesion-containing oligonucleotides have been published (10, 11, 21, 28, 30, 34–39). These studies provide a better understanding of the

\* This work was supported, in whole or in part, by National Institutes of Health Grants R01 ES010375 (to F. P. G. and M. E.) and P01 CA160032 (to M. E.). The authors declare that they have no conflicts of interest with the contents of this article.

The atomic coordinates and structure factors (codes 4YR0, 4YR2, 4YR3, 4YP3, and 4YQW) have been deposited in the Protein Data Bank (<http://www.pdb.org/>).

<sup>1</sup> To whom correspondence should be addressed: Dept. of Biochemistry, Vanderbilt University School of Medicine, 638B Robinson Research Bldg., 2200 Pierce Ave., Nashville, TN 37232-0146. Tel.: 615-322-2261; Fax: 615-322-4349; E-mail: f.guengerich@vanderbilt.edu.

<sup>2</sup> The abbreviations used are: hpol  $\eta$ , human DNA polymerase  $\eta$ ; FAM, 6-carboxyfluorescein; 8-oxoG, 7,8-dihydro-8-oxo-2'-deoxyguanosine; PDB, Protein Data Bank; dCMPNPP, 2'-deoxycytidine-5'-[( $\alpha,\beta$ )-imidazole]triphosphate.

## Arg-61 and Gln-38 Roles in Human Polymerase $\eta$

catalytic mechanism and have yielded valuable information regarding the design of potential drugs against hpol  $\eta$  in the hope of blocking tumor proliferation. The residue Arg-61, located in a short loop region, is highly conserved. Its dynamic movement contributes to the catalytic activity of the enzyme. X-ray crystal structures reveal that after binding the DNA substrate in the absence of an incoming dNTP, the positively charged guanidino moiety of Arg-61 is projected toward the nucleobase of the 5'-overhanging, single-stranded region of template DNA of the template-primer duplex (38). However, following binding of dNTP and divalent metal ions, the side chain of Arg-61 undergoes a rotation and interacts with the  $\alpha$ -phosphate of the incoming dNTP. Interestingly, the side chain of Arg-61 also moves during phosphodiester bond formation to allow enough space for a third divalent metal ion, which interacts with both the  $\alpha$ -phosphate and the oxygen, bridging the  $\alpha$ - and  $\beta$ -phosphates. Thus, Arg-61 can adopt different conformations during each stage of the catalytic reaction cycle. In addition, the reported structures have also indicated that another highly conserved residue near the active site, Gln-38, may play an important role in stabilizing the template base in the nucleotidyl transfer reaction (10, 11, 21, 30, 34, 35, 37).

Site-directed mutagenesis was used in this study to further investigate the roles of Arg-61 and Gln-38 in the catalytic activity. Wild-type and mutant forms of hpol  $\eta$  were analyzed and crystallized with unmodified DNA or DNA containing 8-oxoG. The combined results of the structural and biochemical analysis indicate that the positioning and positive charge of the Arg-61 synergistically contribute to the nucleotidyl transfer reaction in addition to the hydrogen bonding effect of Gln-38 with the template base. When both Arg-61 and Gln-38 were replaced by Ala, polarized water molecules could mimic and partially compensate for the missing wild-type side chains.

### Experimental Procedures

**Materials**—All oligonucleotides were purchased from Integrated DNA Technologies (Coralville, IA), and some were purified by HPLC. dNTPs were from New England Biolabs (Ipswich, MA). PreScission protease was from GE Healthcare. Polyethylene glycol monomethyl ether 2000 (for crystallization) was from Hampton Research (Aliso Viejo, CA).

**Site-directed Mutagenesis, Protein Expression, and Purification**—Wild-type hpol  $\eta$  (residues 1–432, in a pET28a plasmid) was a gift from Dr. Wei Yang (NIDDK, National Institutes of Health, Bethesda, MD). Site-directed mutagenesis was used to make point mutations by the following primers: Q38A, 5'-CATGCGCCGTTGTGGCGTATAAAAAGCTGG-3' and 5'-CCAGCTTTTATACGCCACAACGGCGCATG-3'; Q38L, 5'-CCATGCGCCGTTGTGCTGTATAAAAAGCTGGAAAGG-3' and 5'-CCTTTCCAGCTTTTATACAGCACAACGGCGCATGG-3'; R61A, 5'-CGTTTGGCGTCACCGCCAGCATGTGGGCCGATG-3' and 5'-CATCGGCCACATGCTGGCGGTGACGCCAAACG-3'; R61K, 5'-GTTTGGCGTCACCAAGAGCATGTGGGCCGATGAC-3' and 5'-GTCATCGGCCACATGCTCTTGGTGACGCCAAAC-3'; R61M, 5'-GTTTGGCGTCACCATGAGCATGTGGGCCGATGAC-3' and 5'-GTCATCGGCCACATGCTCATGGTGACGCCA-

AAC-3'. Wild-type and mutant hpol  $\eta$  derivatives were expressed in *Escherichia coli* BL21 (DE3) pLysS cells, followed by purification through a HisTrap HP column (5 ml; GE Healthcare). After removal of the N-terminal His tag by PreScission protease (GE Healthcare), the proteins were purified through a Mono S column (GE Healthcare), eluted with the buffer containing 20 mM sodium MES (pH 6.0), 3 mM dithiothreitol (DTT), 0.1 mM EDTA, 10% glycerol (v/v), and  $\sim$ 350 mM KCl (using a gradient of 250–500 mM KCl). The proteins were used for activity assays after flash freezing in liquid nitrogen and storage at  $-80^\circ\text{C}$ . Proteins were further purified through a Superdex-75 10/300 GL column (GE Healthcare) in 20 mM Tris-HCl buffer (pH 7.5) containing 450 mM KCl and 3 mM DTT (35) to obtain crystals. In addition, the R61M mutant was analyzed with a Superdex-200 10/300 GL column (GE Healthcare) with 20 mM Tris-HCl (pH 7.5) containing 450 mM KCl and 3 mM DTT as well as bovine thyroglobulin (Sigma-Aldrich) and bovine serum albumin (BSA).

**Annealing and Extension Assays**—Primer and template DNA were annealed (1:1 molar ratio) by heating to  $95^\circ\text{C}$  for 5 min and slow cooling to room temperature: (a) 5'-6-carboxyfluorescein (FAM)-CGGGCTCGTAAGCGTCAT-3' and 3'-GCCCGAGCATTTCGCAGTAGTACT-5'; (b) 5'-FAM-CGGGCTCGTAAGCGTCAT-3' and 3'-GCCCGAGCATTTCGCAGTA(8-oxoG)TACT-5'; (c) 5'-FAM-CGGGCTCGTAAGCGTCATC-3' and 3'-GCCCGAGCATTTCGCAGTA(8-oxoG)TACT-5'; (d) 5'-FAM-CGGGCTCGTAAGCGTCATA-3' and 3'-GCCCGAGCATTTCGCAGTA(8-oxoG)TACT-5'; (e) 5'-AGCGTCAT-3' and 3'-TCGCAGTAGTAC-5'; (f) 5'-AGCGTCAT-3' and 3'-TCGCAGTA(8-oxoG)TAC-5'; (g) 5'-FAM-CGGGCTCGTAAGCGTCATC-3' and 3'-GCCCGAGCATTTCGCAGTAGTACT-5'. DNA complexes a–d were used for extension assays; a–c and g were applied in steady-state kinetic assays; a and b were used in pre-steady-state kinetic assays; e and f were used for crystallization. For the extension assays, wild-type hpol  $\eta$  or mutant proteins (25 nM) were incubated with 5  $\mu\text{M}$  FAM-labeled primer-template DNA complex in 40 mM Tris-HCl buffer (pH 7.5), 10 mM DTT, 0.1 mg/ml BSA, 5% glycerol (v/v), 5 mM  $\text{MgCl}_2$ , 100 mM KCl, and 200  $\mu\text{M}$  each dNTP. The reactions were conducted for 0, 2, 5, and 15 min at  $37^\circ\text{C}$ . After stopping the reactions, the products were separated using 18% denaturing polyacrylamide gels (w/v) and visualized using a Typhoon system (GE Healthcare).

**Steady-state Kinetics**—Reactions were conducted by incubating hpol  $\eta$  (2–500 nM), 5  $\mu\text{M}$  FAM-labeled primer-template DNA complex, 40 mM Tris-HCl (pH 7.5) containing 10 mM DTT, 0.1 mg/ml BSA, 5% glycerol (v/v), 5 mM  $\text{MgCl}_2$ , 100 mM KCl, and various amounts of dCTP or dATP at  $37^\circ\text{C}$  for 5 min. After quenching the reactions, products were applied on 18% denaturing polyacrylamide gels (w/v), visualized with a Typhoon system (GE Healthcare), and quantified using ImageJ software (National Institutes of Health). The data were fit to the (hyperbolic) Michaelis-Menten equation with Prism software (GraphPad, La Jolla, CA) (10, 30).

**Pre-steady-state Kinetics**—FAM-labeled primer-template DNA complex (1  $\mu\text{M}$ ) was mixed with wild-type (100 nM) or mutant (500 nM) hpol  $\eta$ , 40 mM Tris-HCl (pH 7.5), 10 mM DTT, 0.1 mg/ml BSA, 5% glycerol (v/v), and 100 mM KCl (Solution A).

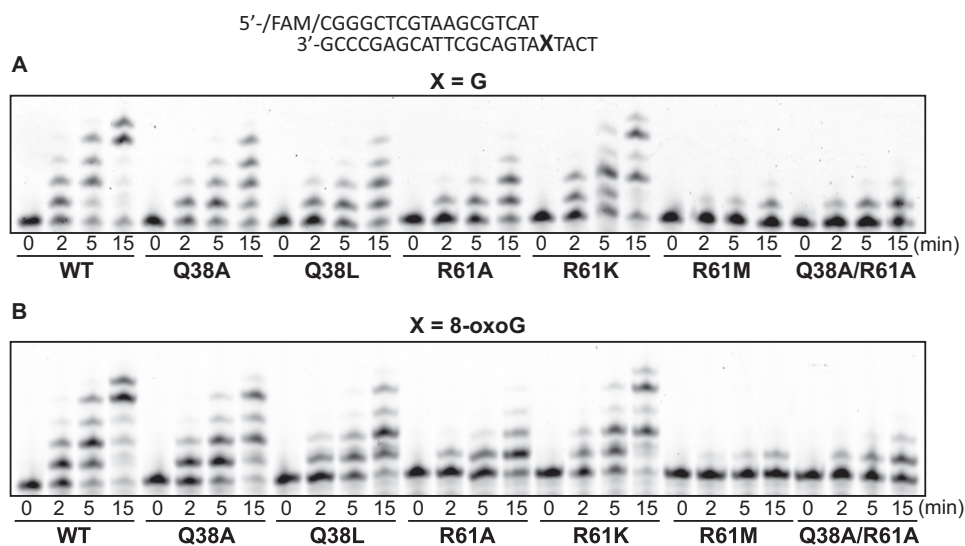


FIGURE 1. **Primer extension assays for bypass of G or 8-oxoG by wild-type or mutant hpol  $\eta$ .** Wild-type or mutant hpol  $\eta$  (25 nM), FAM-labeled primer-template DNA complex (5  $\mu$ M), and a saturating concentration of all four dNTPs (200  $\mu$ M each dNTP) were incubated at 37 °C for 0, 2, 5, and 15 min. The products were separated on denaturing polyacrylamide gels. In *A*, X represents G; in *B*, X represents 8-oxoG.

Solution B contained 1 mM dCTP and 10 mM MgCl<sub>2</sub>. The two solutions were mixed rapidly with a KinTek RP-3 instrument (KinTek Corp., Austin, TX) at 25 °C for 0.005–5 s (the final reaction concentration for wild-type hpol  $\eta$  was 50 nM, and that for mutant hpol  $\eta$  was 250 nM) and stopped by the addition of 0.5 M EDTA. The products were separated with 18% denaturing polyacrylamide gels (w/v) and visualized with a Typhoon system (GE Healthcare). After quantification using ImageJ software, the results were fit to a burst equation using GraphPad Prism:  $y = A(1 - e^{-k_p t}) + k_{ss} E_0 t$ , where  $A$  is the burst amplitude, representing the apparent concentration of the active form of the enzyme,  $k_p$  is the burst rate,  $k_{ss}$  is the steady-state rate, and  $E_0$  is the total enzyme concentration (30, 37, 40).

**Crystallizations**—The hanging drop vapor diffusion technique was used to obtain crystals. DNA complex and protein (1.2:1 molar ratio) were first incubated at room temperature for 10 min, followed by the addition of 0.5  $\mu$ l of 1 M CaCl<sub>2</sub> and concentration by centrifugation through a filter (10 kDa, Millipore). After the addition of 0.5  $\mu$ l of 100 mM dNTP (New England Biolabs), the solution (1  $\mu$ l) was mixed with an equal volume of reservoir solution (100 mM sodium MES (pH 6.0), 5 mM CaCl<sub>2</sub>, and 15–22% (w/v) polyethylene glycol monomethyl ether 2000 (Hampton Research, Aliso Viejo, CA)). The mixture was equilibrated against 500  $\mu$ l of the reservoir solution at 18 °C. Crystals were typically observed after overnight incubation (30, 35).

**X-ray Diffraction Data Collection and Structure Determination**—Crystals were mounted in nylon loops and swiped through a mixture of reservoir solution plus 25% glycerol (v/v), followed by flash-cooling in liquid nitrogen. Diffraction data were collected on the Sector 21-ID-G beamline at the Advanced Photon Source (Life Sciences Collaborative Access Team, Argonne National Laboratory, Argonne, IL). All collected data were integrated and scaled using HKL2000 (41). Structures were determined by molecular replacement phasing using the program Phaser MR (42). Coordinates with Protein

Data Bank (PDB) code 4O3N were used as the search model for R61M·G·dCTP and Q38A/R61A·G·dCTP, those with PDB code 4O3P were used for R61M·8-oxoG·dCTP and Q38A/R61A·8-oxoG·dCTP, and those with PDB code 4O3O were used for R61M·8-oxoG·dATP. PHENIX (43) was applied for refinements, and ARP/ $\omega$  ARP classic (44, 45) and COOT (46) were used for model building. Structural illustrations were generated with the program UCSF Chimera (47).

## Results

**Primer Extension past G or 8-oxoG by Wild-type or Mutant hpol  $\eta$  in the Presence of All Four dNTPs**—The catalytic core (residues 1–432) of hpol  $\eta$  was used in this study because its activity is similar to that of the full-length protein *in vitro* (10). In order to understand the mechanism of dNTP incorporation by hpol  $\eta$ , point mutations were introduced at Arg-61 and Gln-38. In the extension assays, wild-type hpol  $\eta$  bypassed both unmodified template G and 8-oxoG and fully extended the primer in 15 min, whereas mutants R61M and Q38A/R61A partially elongated the primer by inserting at most two nucleotides, indicating that these mutations strongly attenuate the activity of hpol  $\eta$ . In comparison, the mutations Q38A, Q38L, R61A, and R61K only slightly reduced the catalytic activity (Fig. 1, *A* and *B*).

**Steady-state Kinetics of dCTP or dATP Incorporation Opposite G or 8-oxoG by Wild-type and Mutant hpol  $\eta$** —All hpol  $\eta$  mutants used in our study had attenuated efficiency for dCTP insertion opposite unmodified G compared with the wild-type enzyme. The Q38L, R61M, and Q38A/R61A mutants showed 22-, 19-, and 16-fold attenuation in enzyme efficiency, respectively, whereas Q38A, R61A, and R61K showed only small decreases. Even when these mutations were introduced, hpol  $\eta$  still maintained relatively high fidelity opposite G, and the dATP misincorporation frequency for each hpol  $\eta$  was <4% (Fig. 2*A* and Table 1). For dCTP incorporation opposite 8-oxoG (Fig. 2*B* and Table 2), the lowest catalytic efficiencies ( $k_{cat}/K_m$ ) were observed for the Q38L, R61M, and Q38A/R61A mutants

## Arg-61 and Gln-38 Roles in Human Polymerase $\eta$

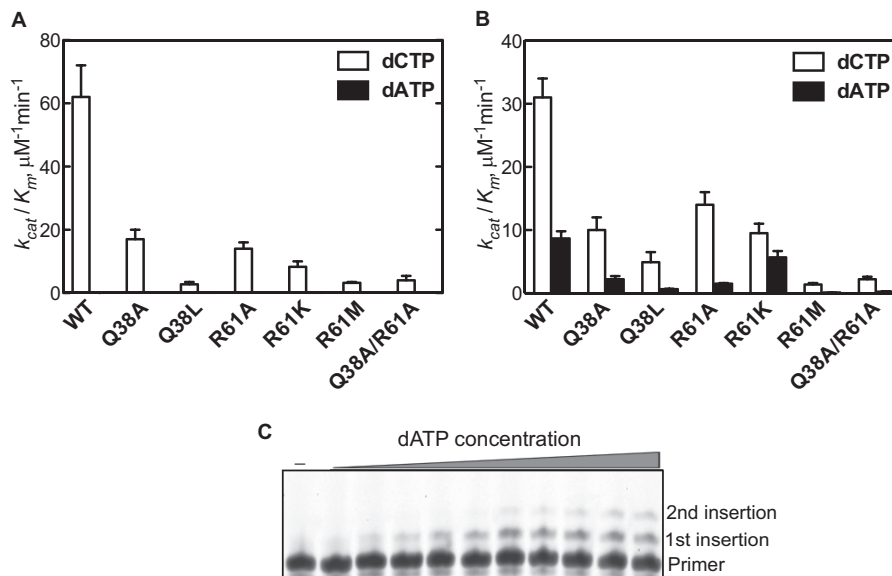


**FIGURE 2. Enzyme efficiencies for dNTP incorporation opposite G or 8-oxoG by wild-type or mutant hpol  $\eta$ .** Enzyme efficiencies ( $k_{\text{cat}}/K_m$ ) were obtained from steady-state kinetic studies by incubating 2–500 nM hpol  $\eta$ , 5  $\mu\text{M}$  FAM-labeled primer-template DNA complex, and varying concentrations of dNTPs at 37 °C for 5 min. After separating the products on denaturing polyacrylamide gels, data were fit to a (hyperbolic) Michaelis-Menten equation using non-linear regression (Prism). Each experiment was conducted at least twice, and *error bars* indicate S.D. *A*, dCTP and dATP incorporation opposite G; *B*, dCTP and dATP incorporation opposite 8-oxoG; *C*, an example (R61A mutant) of second band insertion during a steady-state-kinetic study for dATP incorporation opposite 8-oxoG.

**TABLE 1**

**Steady-state kinetics of incorporation of dCTP and dATP opposite G by wild-type and mutant hpol  $\eta$**

The oligonucleotides used were 5'-FAM-CGGGCTCGTAAGCGTCAT-3' and 3'-GCCCCGAGCATTGCGAGTAGTACT-5'.

hpol $\eta$	dNTP	$K_m$	$k_{\text{cat}}$	$k_{\text{cat}}/K_m$	$f^a$
		$\mu\text{M}$	$\text{min}^{-1}$	$\mu\text{M}^{-1}\text{min}^{-1}$	
WT <sup>b</sup>	dCTP	1.3 ± 0.2	80 ± 3	62 ± 10	
	dATP	92 ± 23	6.0 ± 0.6	0.065 ± 0.018	0.0010
Q38A	dCTP	5.2 ± 0.9	88 ± 5	17 ± 3	
	dATP	103 ± 13	14 ± 1	0.14 ± 0.02	0.0082
Q38L	dCTP	20 ± 5	55 ± 5	2.8 ± 0.7	
	dATP	148 ± 36	15 ± 1	0.10 ± 0.03	0.036
R61A	dCTP	1.5 ± 0.2	21 ± 1	14 ± 2	
	dATP	49 ± 10	0.92 ± 0.09	0.019 ± 0.004	0.0014
R61K	dCTP	8.7 ± 1.7	72 ± 3	8.3 ± 1.7	
	dATP	73 ± 10	8.0 ± 0.4	0.11 ± 0.02	0.013
R61M	dCTP	1.3 ± 0.1	4.2 ± 0.1	3.2 ± 0.3	
	dATP	47 ± 13	0.14 ± 0.01	0.0030 ± 0.0009	0.00094
Q38A/R61A	dCTP	6.5 ± 2.2	26 ± 2	4.0 ± 1.4	
	dATP	78 ± 15	2.1 ± 0.1	0.027 ± 0.005	0.0068

<sup>a</sup> Misinsertion frequency:  $f = (k_{\text{cat}}/K_m)_{\text{dATP}} / (k_{\text{cat}}/K_m)_{\text{dCTP}}$ .

<sup>b</sup> Steady-state kinetic data of dNTP incorporation opposite G by WT hpol  $\eta$  were from Ref. 30. The experimental conditions for WT and hpol  $\eta$  mutants were identical.

(i.e. 4.9, 1.4, and 2.2  $\mu\text{M}^{-1}\text{min}^{-1}$  respectively, compared with 31  $\mu\text{M}^{-1}\text{min}^{-1}$  for wild-type hpol  $\eta$ ). In the study of steady-state kinetics of dATP misinsertion opposite 8-oxoG, a second insertion band was always observed due to the next base T, 3' to 8-oxoG on the template strand (Fig. 2C). To obtain catalytic efficiencies specifically for the insertion step opposite 8-oxoG, the two insertion bands were both included in the quantitation. We reported previously that the dATP insertion frequency was 280-fold higher for wild-type hpol  $\eta$  replicating past 8-oxoG than that for replicating past G (30). For each mutant, dATP was more frequently inserted opposite 8-oxoG than G. Interestingly, all mutants except R61K showed higher fidelity (inserting dCTP instead of dATP) than wild-type hpol  $\eta$  in bypassing 8-oxoG. The R61K

**TABLE 2**

**Steady-state kinetics of incorporation of dCTP and dATP opposite 8-oxoG by wild-type and mutant hpol  $\eta$**

The oligonucleotides used were 5'-FAM-CGGGCTCGTAAGCGTCAT-3' and 3'-GCCCCGAGCATTGCGAGTA(8-oxoG)TACT-5'.

hpol $\eta$	dNTP	$K_m$	$k_{\text{cat}}$	$k_{\text{cat}}/K_m$	$f^a$
		$\mu\text{M}$	$\text{min}^{-1}$	$\mu\text{M}^{-1}\text{min}^{-1}$	
WT <sup>b</sup>	dCTP	2.3 ± 0.2	72 ± 2	31 ± 3	
	dATP	7.6 ± 0.9	66 ± 2	8.7 ± 1.1	0.28
Q38A	dCTP	9.1 ± 1.8	93 ± 8	10 ± 2	
	dATP	14 ± 3	31 ± 2	2.2 ± 0.5	0.22
Q38L	dCTP	13 ± 4	64 ± 7	4.9 ± 1.6	
	dATP	34 ± 4	22 ± 1	0.65 ± 0.08	0.13
R61A	dCTP	1.3 ± 0.2	18 ± 1	14 ± 2	
	dATP	11 ± 1	17 ± 0.4	1.5 ± 0.1	0.11
R61K	dCTP	8.4 ± 1.3	80 ± 4	9.5 ± 1.5	
	dATP	12 ± 2	68 ± 2	5.7 ± 1.0	0.60
R61M	dCTP	1.7 ± 0.3	2.3 ± 0.1	1.4 ± 0.2	
	dATP	15 ± 2	1.7 ± 0.1	0.11 ± 0.02	0.079
Q38A/R61A	dCTP	7.7 ± 1.3	17 ± 1	2.2 ± 0.4	
	dATP	29 ± 8	6.9 ± 0.5	0.24 ± 0.07	0.11

<sup>a</sup> Misinsertion frequency:  $f = (k_{\text{cat}}/K_m)_{\text{dATP}} / (k_{\text{cat}}/K_m)_{\text{dCTP}}$ .

<sup>b</sup> Steady-state kinetic data of dNTP incorporation opposite 8-oxoG by WT hpol  $\eta$  were from Ref. 30. The experimental conditions were the same for WT and mutant forms of hpol  $\eta$ .

mutant, consistent with a previous report (21), had a higher misincorporation frequency (0.60, compared with 0.28 for wild-type hpol  $\eta$ ) (Fig. 2B and Table 2).

**Pre-steady-state Kinetics of dCTP Incorporation Opposite G or 8-oxoG by Wild-type and Mutant hpol  $\eta$** —In the pre-steady-state kinetic analysis of dCTP insertion opposite G, the burst rates for R61M and Q38A/R61A were 2.6- and 5.9-fold lower than that for wild-type hpol  $\eta$  (Fig. 3 and Table 3). A similar trend was observed for bypass of 8-oxoG, with 90  $\text{s}^{-1}$  for wild-type, 35  $\text{s}^{-1}$  for R61M, and 53  $\text{s}^{-1}$  for Q38A/R61A. In the bypass of G, the burst amplitude of wild type was nearly 100% of the estimated enzyme concentration, but the burst amplitudes for R61M and Q38A/R61A were only 21 and 16%, respectively, suggesting the presence of either inactive enzymes or multiple

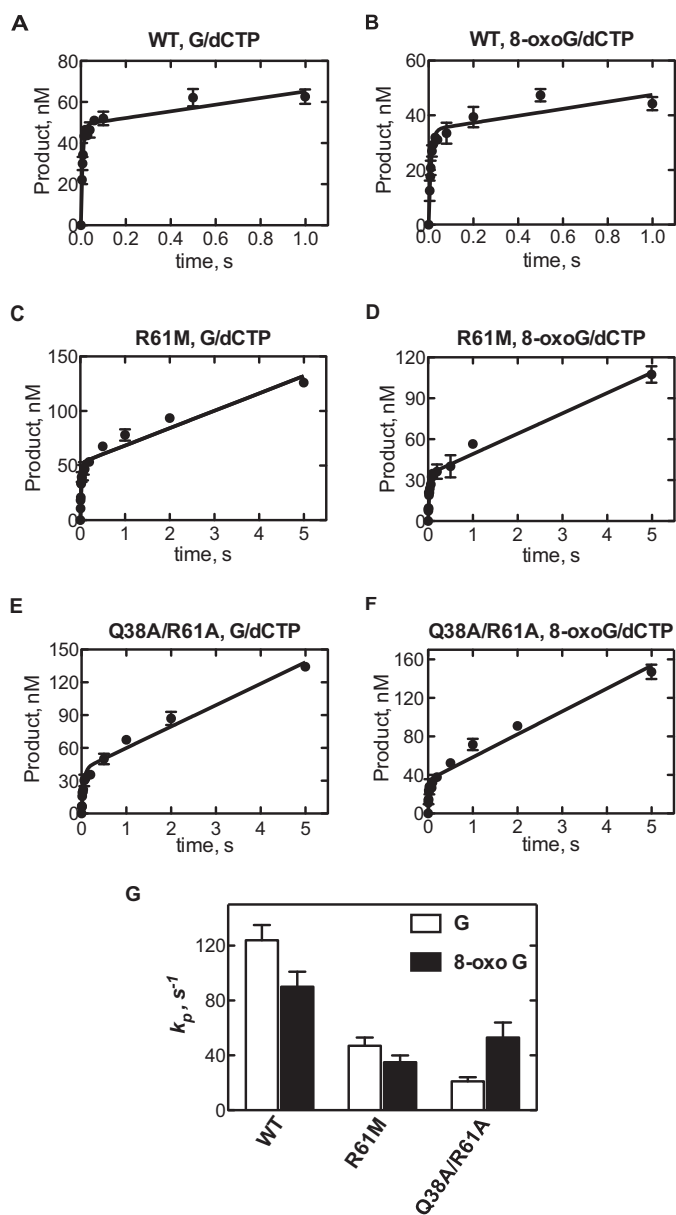


**FIGURE 3. Pre-steady-state kinetic analysis of dCTP incorporation opposite G or 8-oxoG by wild-type or mutant hpol  $\eta$ .** A mixture of 1  $\mu$ M FAM-labeled DNA complex and 100 nM wild-type or 500 nM mutant hpol  $\eta$  was mixed with an equal volume of solution containing 1 mM dCTP and 10 mM MgCl<sub>2</sub> for 0.005–5 s at 25 °C (wild-type hpol  $\eta$  was 50 nM; mutant was 250 nM in the reactions), followed by the addition of quenching solution (0.5 M EDTA) and separation of products on denaturing polyacrylamide gels. The quantified data were fit to a burst equation,  $y = A(1 - e^{-k_p t}) + k_{ss}E_{0t}$ . Each experiment was conducted twice, and error bars represent S.D. A, wild-type hpol  $\eta$  (WT) incorporation of dCTP opposite G; B, wild-type hpol  $\eta$  (WT) incorporation of dCTP opposite 8-oxoG; C, mutant R61M incorporation of dCTP opposite G; D, mutant R61M incorporation of dCTP opposite 8-oxoG; E, mutant Q38A/R61A incorporation of dCTP opposite G; F, mutant Q38A/R61A incorporation of dCTP opposite 8-oxoG; G, comparison of the burst rates ( $k_p$ ) for dCTP incorporation opposite G and 8-oxoG.

conformations in mutant·DNA·dNTP ternary complexes (48). For the bypass of 8-oxoG, the burst amplitudes were  $\sim$ 14% for each hpol  $\eta$  mutant and  $\sim$ 70% for wild-type hpol  $\eta$ . Notably, for each individual enzyme, the burst amplitude for incorporation opposite G was always larger than that for 8-oxoG, suggesting that non-productive forms are more prominent in the presence of 8-oxoG (48) (Table 3).

**TABLE 3**

**Burst kinetics of incorporation of dCTP opposite G and 8-oxoG**

The oligonucleotides used were 5'-FAM-CGGGCTCGTAAGCGTCAT-3' and 3'-GCCCGAGCATTTCGAGTAGTACT-5'; 5'-FAM-CGGGCTCGTAAGCGTCAT-3' and 3'-GCCCGAGCATTTCGAGTA(8-oxoG)TACT-5'.

hpol $\eta^a$	Template	$k_p$ $s^{-1}$	$k_{ss}$ $s^{-1}$	Burst amplitude $nM$
WT	G	124 $\pm$ 11	0.32 $\pm$ 0.05	49 $\pm$ 1
	8-oxoG	90 $\pm$ 11	0.26 $\pm$ 0.06	35 $\pm$ 1
R61M	G	47 $\pm$ 6	0.064 $\pm$ 0.004	52 $\pm$ 2
	8-oxoG	35 $\pm$ 5	0.060 $\pm$ 0.003	34 $\pm$ 2
Q38A/R61A	G	21 $\pm$ 3	0.078 $\pm$ 0.004	40 $\pm$ 2
	8-oxoG	53 $\pm$ 11	0.095 $\pm$ 0.004	35 $\pm$ 2

<sup>a</sup> The final enzyme concentrations were 50 nM WT hpol  $\eta$  and 250 nM R61M and Q38A/R61A.

**Post-G or -8-oxoG Synthesis by Wild-type or Mutant hpol  $\eta$** —The ternary crystal structure shows that 8-oxoG formed a Watson-Crick pair with an incoming dCTP analog in the presence of wild-type hpol  $\eta$  (PDB code 4O3P) (30). The question can be raised as to whether the presence of an 8-oxoG:C pair affects primer extension by wild-type or mutant hpol  $\eta$ . In the presence of all four dNTPs, wild-type hpol  $\eta$  fully extended the primer beyond the 8-oxoG:C pair in 15 min, and the Q38A, Q38L, R61A, and R61K mutants elongated the primer at slightly slower rates, but only part of the primer was extended (by one nucleotide) by the R61M and Q38A/R61A mutants (Fig. 4A).

To further investigate primer extension post-8-oxoG, steady-state kinetic analysis was applied for the next base (dATP) insertion beyond an 8-oxoG:C pair, as well as a G:C pair as a control. Consistent with the observation in Fig. 4A, the catalytic efficiencies ( $k_{cat}/K_m$ ) for dATP insertion post-8-oxoG were much lower for R61M (1.8  $\mu$ M<sup>-1</sup> min<sup>-1</sup>) or Q38A/R61A (1.2  $\mu$ M<sup>-1</sup> min<sup>-1</sup>) compared with wild-type hpol  $\eta$  (47  $\mu$ M<sup>-1</sup> min<sup>-1</sup>). Interestingly, both wild-type hpol  $\eta$  and the two mutants had similar  $k_{cat}/K_m$  values for dATP incorporation post-G and -8-oxoG, indicating that 8-oxoG does not affect next base insertion by hpol  $\eta$ , even with mutations at Arg-61 or Gln-38 (Table 4).

Because wild-type or mutant hpol  $\eta$  may incorporate dATP opposite 8-oxoG, extension assays beyond the 8-oxoG:A pair were also studied. The extension pattern beyond an 8-oxoG:A pair was very similar to that beyond an 8-oxoG:C pair for wild-type hpol  $\eta$  or either mutant, indicating that the mismatched 8-oxoG:A pair does not dramatically affect subsequent dNTP insertion (Fig. 4B).

**X-ray Crystallography of Mutant hpol  $\eta$  Inserting dCTP Opposite G**—In order to further understand the roles of Arg-61 and Gln-38 in bypassing unmodified G, crystal structures of R61M·G·dCTP (R61M mutant incorporating dCTP opposite unmodified template G) and Q38A/R61A·G·dCTP were obtained in the presence of Ca<sup>2+</sup>, which does not support nucleotidyl transfer reactions (Table 5). Electron density for the active site of each ternary complex is shown in Fig. 5. Similar to the structure of the wild-type hpol  $\eta$ ·G·dCTP complex, hpol  $\eta$  mutants R61M and Q38A/R61A provided a scaffold for the incoming dCTP and template G to form a Watson-Crick base pair (Fig. 6). The distances were 3.8 and 4.1 Å from the 3'-OH of T of the primer strand to P $\alpha$  of the incoming dCTP in the

## Arg-61 and Gln-38 Roles in Human Polymerase $\eta$

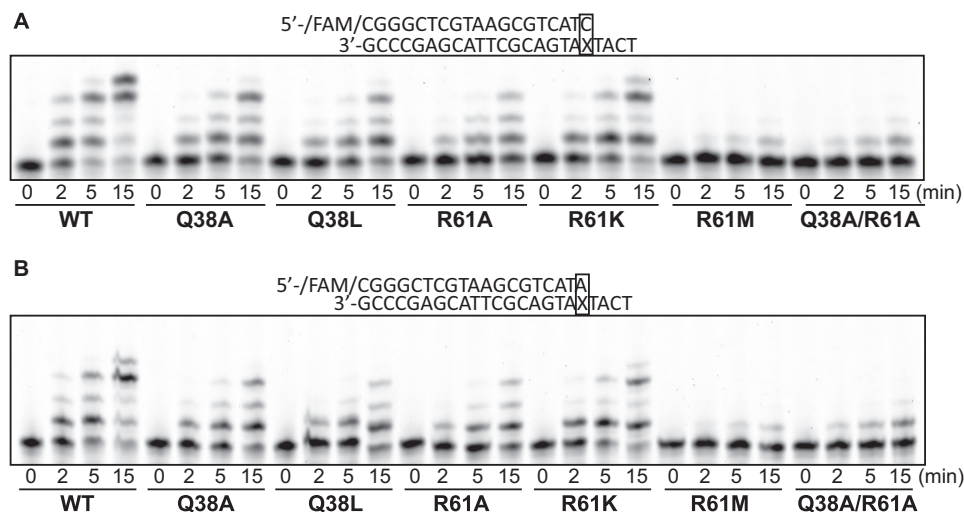


FIGURE 4. **Extension of primer beyond an 8-oxoG:C or 8-oxoG:A pair by wild-type or mutant hpol  $\eta$ .** A FAM-labeled 19-mer primer and 23-mer template were annealed, with 8-oxoG located at position 19 from the 3'-end in the template strand. The DNA complex ( $5 \mu\text{M}$ ) was incubated with a 25 nM concentration of each enzyme and all four dNTPs ( $200 \mu\text{M}$  each dNTP) at  $37^\circ\text{C}$  for 0, 2, 5, and 15 min, followed by separation of products on denaturing polyacrylamide gels. A, C was at the 3'-end of the primer and opposite 8-oxoG. B, A was at the 3'-end of the primer and opposite 8-oxoG.

**TABLE 4**

### Steady-state kinetics of next base (dATP) insertion post-unmodified G or 8-oxoG by wild-type and mutant hpol $\eta$

The oligonucleotides used were 5'-FAM-CGGGCTCGTAAGCGTCATC-3' and 3'-GCCCGAGCATTGCGAGTACT-5'; 5'-FAM-CGGGCTCGTAAGCGTCATC-3' and 3'-GCCCGAGCATTGCGAGTACT-5'; 5'-FAM-CGGGCTCGTAAGCGTCATC-3' and 3'-GCCCGAGCATTGCGAGTACT-5'.

hpol $\eta$	Template	$K_m$	$k_{\text{cat}}$	$k_{\text{cat}}/K_m$
		$\mu\text{M}$	$\text{min}^{-1}$	$\mu\text{M}^{-1} \text{min}^{-1}$
WT	Post-G	$2.0 \pm 0.5$	$85 \pm 7$	$43 \pm 11$
	Post-8-oxoG	$1.8 \pm 0.2$	$84 \pm 2$	$47 \pm 5$
R61M	Post-G	$2.5 \pm 0.2$	$6.0 \pm 0.1$	$2.4 \pm 0.2$
	Post-8-oxoG	$1.9 \pm 0.3$	$3.5 \pm 0.1$	$1.8 \pm 0.3$
Q38A/R61A	Post-G	$15 \pm 3$	$24 \pm 1$	$1.6 \pm 0.3$
	Post-8-oxoG	$17 \pm 2$	$20 \pm 1$	$1.2 \pm 0.2$

R61M-G·dCTP and Q38A/R61A-G·dCTP complexes respectively, compared with 3.3 or 3.5 Å (two conformations) for wild-type hpol  $\eta$  (30).

Arg-61 of wild-type hpol  $\eta$  engages in favorable Coulombic interaction with the  $\alpha$ -phosphate of the incoming dCTP. The electrostatic force was lost after mutating it to the hydrophobic Met, although the size of the side chain was similar to Arg. Interestingly, in the ternary Q38A/R61A-G·dCTP complex, one water molecule was located above the base ring of dCTP and likely to form a lone pair- $\pi$  or H- $\pi$  interaction with the nucleobase (Fig. 6) (49).

In the minor groove of the wild-type ternary complex, the  $\text{N}^\epsilon$  atom of Gln-38 connected with N3 of the template G through a hydrogen bond and a water molecule-bridged  $\text{O}^\epsilon$  of Gln-38 and N2 of G, thus stabilizing the template G to form a base pair with the incoming dCTP. When Gln-38 was mutated to Ala, these interactions were disrupted, and the bridging water molecule was not present in the Q38A/R61A-G·dCTP structure (Fig. 6).

**X-ray Crystallography of Mutant hpol  $\eta$  Inserting dCTP Opposite 8-oxoG**—To investigate the roles of Arg-61 and Gln-38 in bypassing 8-oxoG, mutant hpol  $\eta$  was crystallized with dCTP opposite 8-oxoG in the presence of  $\text{Ca}^{2+}$ . Fourier ( $2F_o - F_c$ ) sum electron density maps are shown in Fig. 5. Similar to the structures depicting dCTP insertion opposite unmodified G, wild-type hpol  $\eta$  and the mutants provided a

scaffold for dCTP pairing with 8-oxoG in the Watson-Crick geometry, with 8-oxoG in the *anti* conformation (Fig. 7). The distances between the primer terminal 3'-OH and the  $\text{P}^\alpha$  of dCTP were 3.2 or 3.4 Å in the complex with wild-type hpol  $\eta$  (30), 3.3 or 3.9 Å with the R61M mutant, and 3.9 Å with Q38A/R61A, respectively.

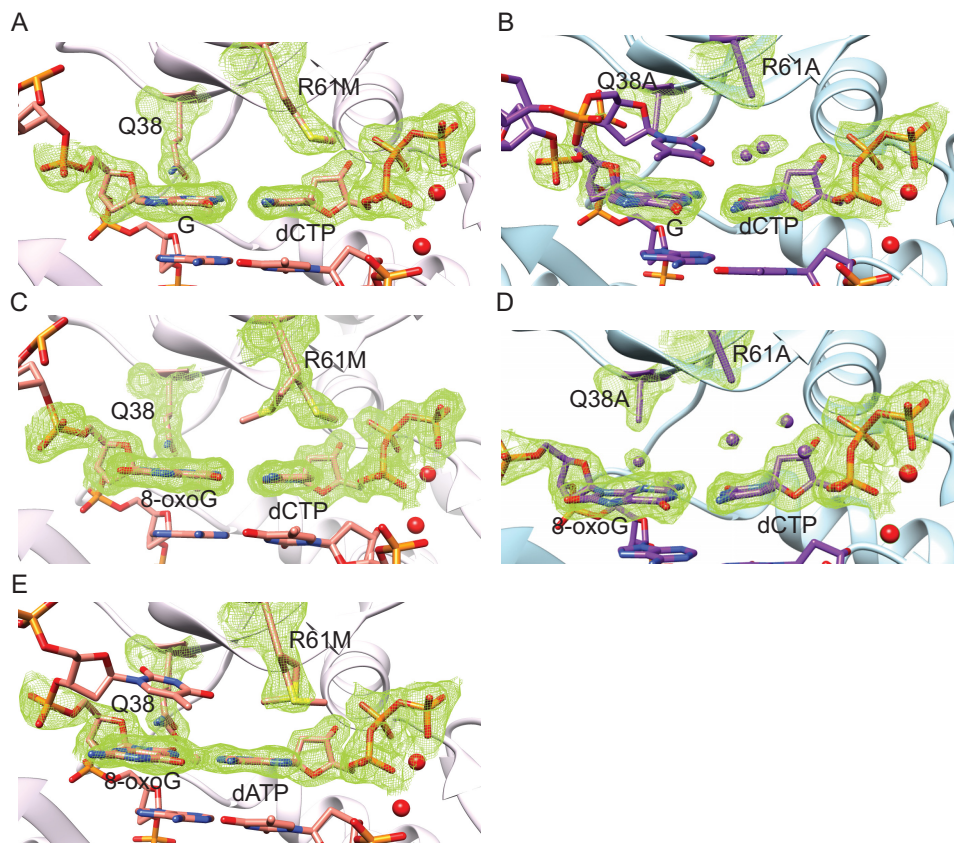
Similar to dCTP insertion opposite G by wild-type hpol  $\eta$ , the side chain of Arg-61 is involved in an electrostatic interaction with the  $\alpha$ -phosphate of dCTP in the wild-type hpol  $\eta$ -8-oxoG·dCTP complex, but this interaction was destroyed when replacing Arg-61 with Met. Interestingly, when Arg-61 was mutated to Ala, water molecules were lodged on top of dCTP. One of the water molecules was on top of the nucleobase of the dCTP, whereas the position of the other matched that of  $\text{N}^\gamma$  of Arg-61 from the wild-type hpol  $\eta$ -8-oxoG·dCTP complex, allowing it to donate a hydrogen bond to the  $\alpha$ -phosphate of the incoming dCTP (Fig. 7).

In the minor groove of the wild-type ternary complex,  $\text{N}^\epsilon$  of Gln-38 was engaged in a hydrogen bond with N3 of 8-oxoG. After superimposition, a water molecule in the Q38A/R61A-8-oxoG·dCTP complex was observed near the  $\text{N}^\epsilon$  of Gln-38 in the wild-type hpol  $\eta$ -8-oxoG·dCTP complex. Further investigation revealed a hydrogen bonding interaction between this water and the N3 of 8-oxoG. In addition, in the wild-type hpol  $\eta$ -8-oxoG·dCTP complex, a water molecule bridged both the  $\text{O}^\epsilon$  of Gln-38 and N2 of 8-oxoG by hydrogen bonds. This bridging water hydrogen-bonds with the  $\text{N}^\epsilon$ -mimicking water as well as N2 of 8-oxoG in the Q38A/R61A-8-oxoG·dCTP complex (Fig. 7).

**X-ray Crystallography of Mutant hpol  $\eta$  Inserting dATP Opposite 8-oxoG**—To explore the role of Arg-61 in the fidelity of hpol  $\eta$ , we crystallized the hpol  $\eta$  R61M mutant with dATP opposite 8-oxoG. Similar to the wild-type hpol  $\eta$ -8-oxoG·dATP complex, 8-oxoG adopted the *syn* conformation and formed a Hoogsteen pair with the incoming dATP when Arg-61 was mutated to Met. The distance from the 3'-OH of the primer end to  $\text{P}^\alpha$  of dATP was 3.7 Å, com-

**TABLE 5**  
Crystal data, data collection parameters, and structure refinement statistics

Complex	R61M 8-oxoG-dCTP	R61M 8-oxoG-dATP	R61M G-dCTP	Q38A/R61A 8-oxoG-dCTP	Q38A/R61A G-dCTP
<b>Data collection</b>					
Wavelength (Å)	0.97856	0.97856	0.97856	0.97856	0.97856
Space group	$P6_1$	$P6_1$	$P6_1$	$P6_1$	$P6_1$
Resolution (Å)	50.00-1.78 (1.81-1.78) <sup>b</sup>	50.00-1.95 (1.98-1.95)	50.00-2.00 (2.03-2.00)	50.00-1.89 (1.92-1.89)	50.00-2.06 (2.10-2.06)
Unit cell $a = b, c$ (Å)	98.73, 82.45	98.97, 82.18	98.71, 81.95	98.77, 81.97	99.24, 82.38
Unique reflections	43,702 (2,144)	33,388 (1,642)	30,423 (1,496)	36,455 (1,805)	28,389 (1,229)
Completeness (%)	99.7 (98.6)	99.9 (99.6)	98.7 (98.1)	99.9 (100)	99.2 (85.6)
$I/\sigma(I)$	13.1 (1.87)	21.0 (1.65)	12.3 (2.23)	14.7 (2.21)	10.2 (1.29)
Wilson $B$ -factor (Å <sup>2</sup> )	19.5	27.5	20.3	23.8	26.2
$R$ -merge <sup>a</sup>	0.094 (0.793)	0.080 (0.775)	0.121 (0.813)	0.087 (0.793)	0.149 (0.964)
Redundancy	5.5 (4.4)	5.5 (4.4)	5.8 (5.7)	5.7 (5.7)	5.5 (3.9)
<b>Refinement</b>					
$R$ -work	0.172 (0.282)	0.168 (0.242)	0.176 (0.235)	0.169 (0.245)	0.174 (0.253)
$R$ -free	0.213 (0.347)	0.218 (0.310)	0.219 (0.262)	0.216 (0.311)	0.227 (0.328)
No. of atoms					
Protein/DNA	3260/409	3236/384	3294/367	3235/363	3293/415
dNTP/Ca <sup>2+</sup>	28/2	30/2	28/2	28/2	28/2
H <sub>2</sub> O/glycerol	507/12	404/12	411/0	406/12	302/12
Protein residues	422	423	424	424	427
$B$ -factor (Å)					
Average	23.6	30.6	24.6	28.3	29.7
Protein/DNA	22.4/25.8	29.2/36.6	23.4/29.2	26.8/33.5	28.9/33.5
dNTP/Ca <sup>2+</sup>	13.5/11.5	31.7/28.8	13.0/14.1	18.6/16.7	20.3/19.7
Water/glycerol	29.7/24.0	36.1/33.4	31.7/0	36.2/31.4	33.6/27.7
Root mean square deviations					
Bonds (Å)	0.008	0.008	0.009	0.017	0.008
Angles (degrees)	1.2	1.1	1.2	1.6	1.1
Ramachandran					
Favored (%)	98.34	97.18	97.88	96.94	97.41
Allowed (%)	1.66	2.59	1.65	3.06	2.12
Outliers (%)	0.00	0.23	0.47	0.00	0.47
PDB code	4YR0	4YR2	4YR3	4YP3	4YQW

<sup>a</sup> Data shown in parentheses are from the highest resolution shell.<sup>b</sup>  $R$ -merge:  $R$  linear =  $\text{SUM}(\text{ABS}(I - \langle I \rangle)) / \text{SUM}(I)$ .**FIGURE 5. Electron density maps for the active sites of mutant ternary complexes.** The Fourier ( $2F_o - F_c$ ) sum electron density is at the  $1\sigma$  threshold. A, R61M-G-dCTP; B, Q38A/R61A-G-dCTP; C, R61M-8-oxoG-dCTP; D, Q38A/R61A-8-oxoG-dCTP; E, R61M-8-oxoG-dATP. The metal ions (Ca<sup>2+</sup>) are shown in red in each panel.

## Arg-61 and Gln-38 Roles in Human Polymerase $\eta$

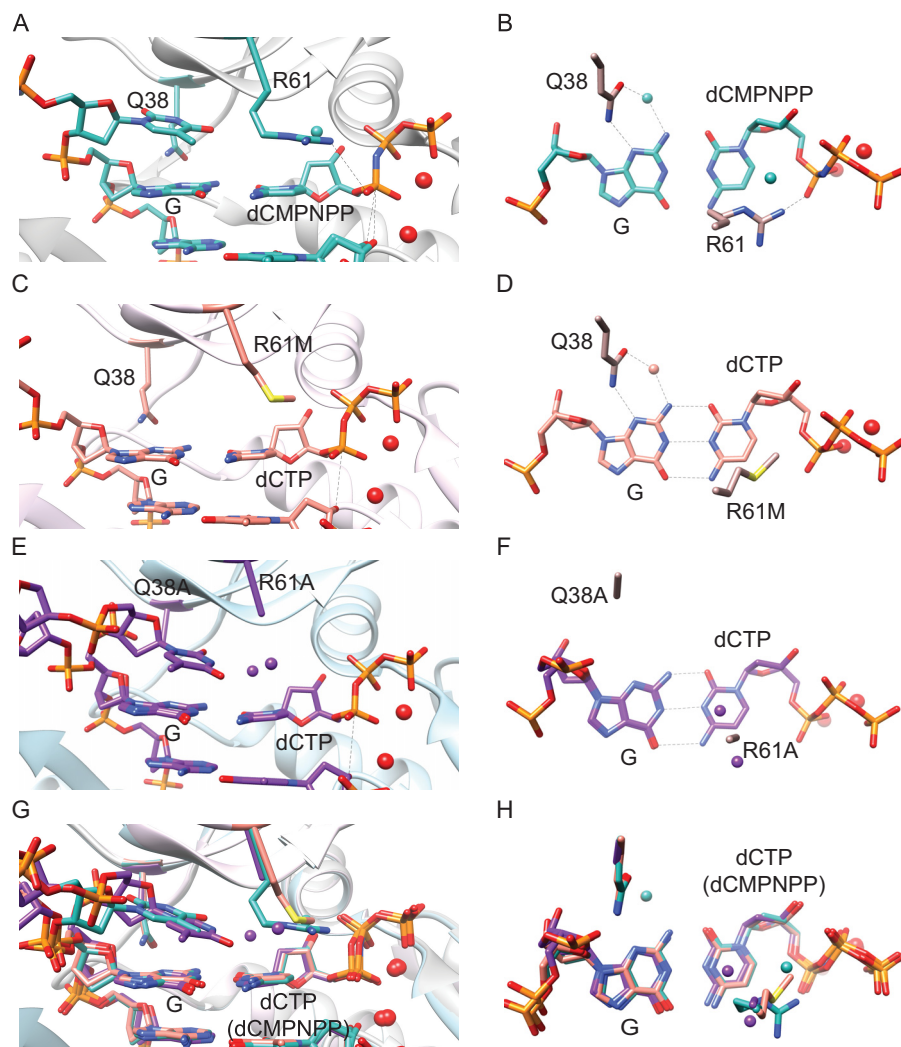


FIGURE 6. **Active site views of dCTP insertion opposite unmodified G by wild-type and mutant hpol  $\eta$ .** A, C, E, and G, views from the major groove side; B, D, F, and H, views of from the top of base pairings. A and B, wild-type hpol  $\eta$ -G-dCMPNPP (PDB 4O3N); C and D, R61M-G-dCTP; E and F, Q38A/R61A-G-dCTP; G and H, superimposed structures of wild-type hpol  $\eta$ , R61M, and Q38A/R61A with the incoming dCTP opposite template G. The metal ions ( $\text{Mg}^{2+}$  in A and B;  $\text{Ca}^{2+}$  in C-H) are represented in red in each panel.

pared with 3.1 or 3.3 Å in the complex with wild-type hpol  $\eta$  (30) (Fig. 8).

The methionine side chain in the point mutant R61M exhibited two conformations in the ternary structure. One of the conformations partially superimposed with the side chain of Arg-61 in the wild-type hpol  $\eta$ -8-oxoG-dATP complex. However, due to the hydrophobic nature of the Met side chain, the electrostatic interaction seen in the wild-type complex with the incoming dATP was lost. The  $\text{N}^\epsilon$  of Gln-38 from either wild-type or R61M mutant hpol  $\eta$  donated a hydrogen bond to the O8 atom of 8-oxoG in the minor groove (Fig. 8).

**Multimeric Forms of hpol  $\eta$** —Wild-type hpol  $\eta$  and the mutants R61M and Q38A/R61A were purified by gel filtration chromatography (Superdex-75 10/300 GL) prior to crystallization. Two distinct peaks, eluting with  $t_R$  of  $\sim 8.1$  and 11.3 ml, were observed in the chromatogram in each case, suggesting the presence of proteins with different molecular masses (Fig. 9A). The second peak was eluted with the molecular mass of monomeric hpol  $\eta$ , as established using the standards BSA (67 kDa) and ovalbumin (43 kDa). The proteins from the two peaks

had the same mobility in SDS-PAGE (data not shown), indicating that the protein in the first peak was a multimeric form of hpol  $\eta$ . The R61M mutant had the largest ratio of peak 1 (multimer) over peak 2 (monomer) (Fig. 9A), and kinetic assays with minimal protein dilution following the chromatography (final dilution ratio 1:4 (v/v) for the reaction) were used to measure their catalytic activities (burst phase, pre-steady state). The protein from peak 2 (monomer) showed a 1.5-fold higher burst rate compared with that from peak 1 (multimer) for dCTP insertion opposite template G. The burst amplitudes were 65 and 202 nM (compared with the input concentrations of 566 and 772 nM for the peak 1 and 2 proteins), respectively. In addition, both peaks of the R61M mutant were crystallized with DNA and incoming dCTP with no dramatic structural differences (data not shown). To characterize the multimeric composition, the mutant R61M, as well as two markers, thyroglobulin (670 kDa) and BSA (67 kDa), were used to calibrate a Superdex-200 10/300 GL gel filtration column. The mutant enzyme was eluted in a peak corresponding to monomeric hpol  $\eta$ , a broad peak with molecular mass in the range of 400–600

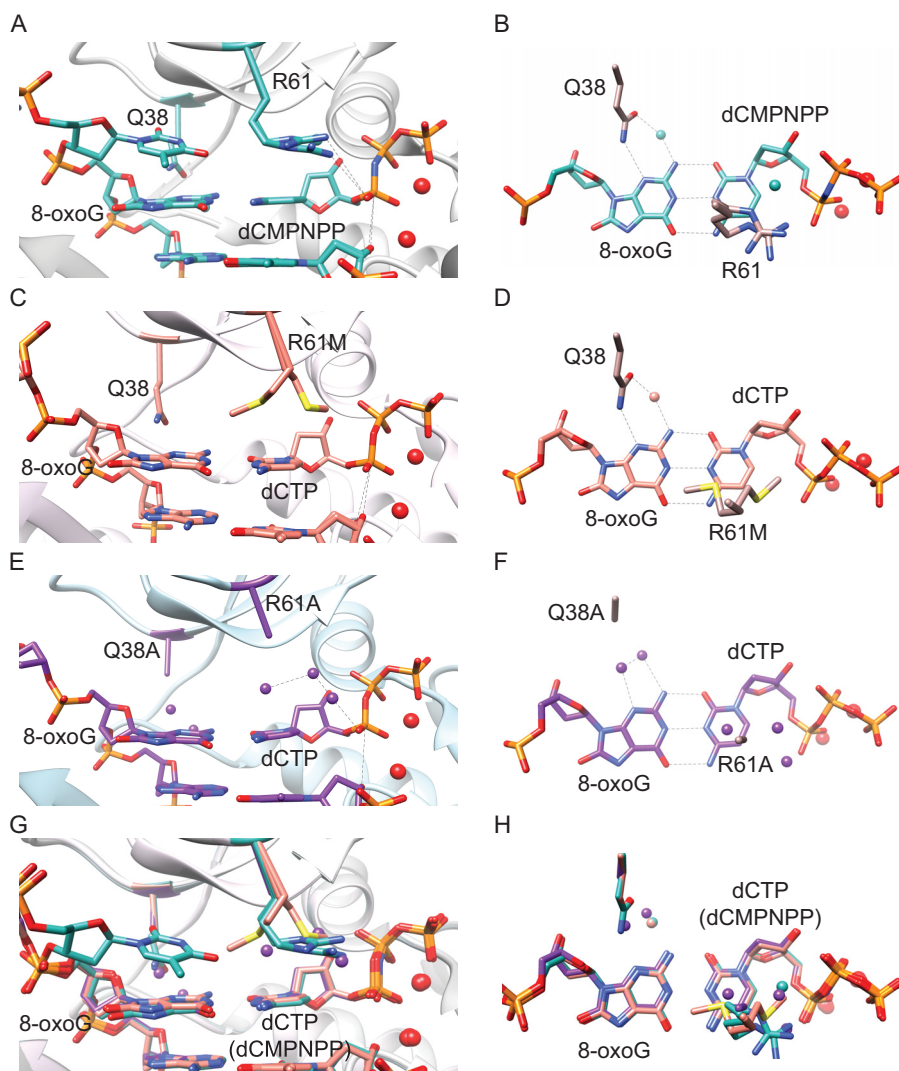


FIGURE 7. Active site views of dCTP insertion opposite 8-oxoG by wild-type and mutant hpol  $\eta$ . A, C, E, and G are views of active sites from the major groove side; base pairings from the top are shown in B, D, F, and H. A and B, wild-type hpol  $\eta$ : 8-oxoG·dCMPNPP (PDB 4O3P); C and D, R61M·8-oxoG·dCTP; E and F, Q38A/R61A·8-oxoG·dCTP; G and H, superimposed structures of wild-type hpol  $\eta$ , R61M, and Q38A/R61A with the incoming dCTP opposite 8-oxoG. The metal ions ( $Mg^{2+}$  in A and B;  $Ca^{2+}$  in C–H) are shown in red.

kDa, and the void peak, indicating the presence of an even higher fold ensemble (Fig. 9B).

## Discussion

The fidelity of some DNA polymerases is determined largely by a single key residue. For example, Arg-332 in the archbacterial *Sulfolobus solfataricus* Y-family DNA polymerase Dpo4 directly interacts with the O8 atom of 8-oxoG and determines its fidelity in the bypass of 8-oxoG (50). Structures of hpol  $\eta$  show that two highly conserved residues, Arg-61 and Gln-38, are important in the catalytic reaction (10, 11, 21, 28, 30, 34–39). In order to delineate their roles for the activity and fidelity of hpol  $\eta$ , we mutated the two residues to amino acids with different side chain properties. The unmodified G and a common DNA lesion, 8-oxoG, were used in DNA templates in our study.

The misincorporation frequencies of wild-type and hpol  $\eta$  mutants for dATP insertion opposite unmodified G were very small, all <4%, as judged from the steady-state kinetic assay

results. However, the misincorporation frequency was increased 36-fold for mutant Q38L, 13-fold for R61K, 8-fold for Q38A, and 7-fold for Q38A/R61A compared with that for wild-type hpol  $\eta$ , whereas mutants R61A and R61M had misincorporation frequencies similar to that of the wild-type protein in incorporating dATP opposite G (Fig. 2A and Table 1). On the other hand, because 8-oxoG can readily form a *syn* conformation due to a steric effect and pair with A, the dATP insertion frequency was increased 280-fold for wild-type hpol  $\eta$  compared with that opposite unmodified G (30). Interestingly, mutant R61K had the highest misincorporation frequency (0.60) for dATP insertion opposite 8-oxoG, whereas R61M had the lowest value (0.079) compared with wild-type hpol  $\eta$  (0.28). The other mutants had slightly reduced misincorporation frequency (Fig. 2B and Table 2). In addition, previous reports also showed that the template base/lesion as well as the flanking sequence also affected the misincorporation frequency for wild-type or mutant hpol  $\eta$  (21, 51). Altogether, we conclude that active site residues, the template base/lesion, and the flank-

## Arg-61 and Gln-38 Roles in Human Polymerase $\eta$

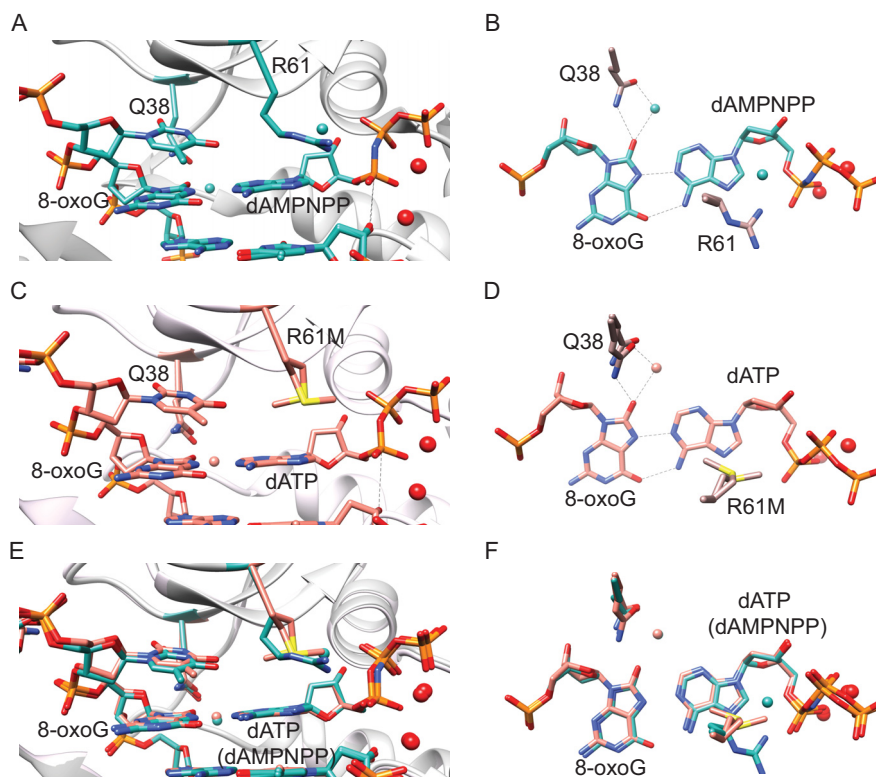


**FIGURE 8. Active site views of dATP misinsertion opposite 8-oxoG by wild-type and mutant hpol  $\eta$ .** *A, C, and E*, active site views from the major groove side. *B, D, and F* show base pairings from the top. *A and B*, wild-type hpol  $\eta$ ·8-oxoG·dAMPNPP (PDB code 4O3O); *C and D*, R61M·8-oxoG·dATP; *E and F*, superimposed structures of wild-type hpol  $\eta$  and the R61M mutant with incoming dATP opposite template 8-oxoG. Metal ions ( $Mg^{2+}$  in *A* and *B*;  $Ca^{2+}$  in *C* and *D*) are shown in red.

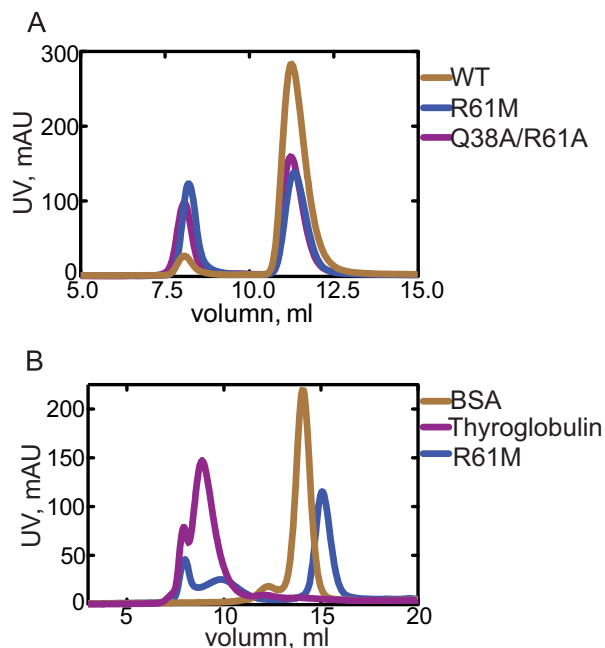


**FIGURE 9. Gel filtration chromatography of wild-type and mutant hpol  $\eta$ .** *A*, wild-type and mutant hpol  $\eta$  were chromatographed on a Superdex-75 10/300 GL gel filtration column. *B*, hpol  $\eta$  R61M mutant plus two standard protein markers, thyroglobulin (670 kDa) and BSA (67 kDa), were loaded on a Superdex-200 10/300 GL gel filtration column, respectively. UV absorbance was monitored at 280 nm.

ing DNA sequence synergistically determine the misincorporation frequency of hpol  $\eta$ .

It was unexpected that the R61A mutant would be more active than R61M; however, x-ray crystal structures of the cor-

responding complexes provide a potential explanation. Polarized water molecules mimic the side chain of Arg-61 and partially compensate for its functions in the R61A mutant. In order to understand how these water molecules participate in the nucleotidyl transfer reaction, the Q38A/R61A·8-oxoG·dCTP complex was compared with the other reported wild-type hpol  $\eta$  structures. A third metal ion ( $Mg^{2+}$ ) has been reported to be involved in the catalytic process, whereas the side chain of Arg-61 of wild-type hpol  $\eta$  adopted the conformation facing toward the major groove (Fig. 10A) (34). After superimposition, the water interacting with the  $\alpha$ -phosphate in the Q38A/R61A·8-oxoG·dCTP complex partially overlapped with a water molecule coordinating with the third  $Mg^{2+}$  (Fig. 10, *B* and *C*). Therefore, the water in the mutant hpol  $\eta$  may not only play a role in mimicking the missing side chain of Arg-61 in the ground state but may also interact with the third metal ion during the catalytic process.

Because  $H_2O$  and monovalent  $Na^+$  may look very similar in electron density maps (52), close investigation of the coordination, occupancy, and *B* factor was conducted (for those water molecules). In particular, the water molecule on top of the base ring of the incoming dCTP was of interest. This water is 2.9 Å from the centroid of the aromatic ring in the Q38A/R61A·G·dCTP complex, and the corresponding distance in the Q38A/R61A·8-oxoG·dCTP complex is 3.1 Å, indicating the possibility of the formation of a lone pair- $\pi$  or H- $\pi$  interaction between  $H_2O$  and the base ring (49). To distinguish  $H_2O$  from a monovalent metal ion, the former was replaced by a  $Na^+$  ion with half-occupancy in the Q38A/R61A·8-oxoG·dCTP model

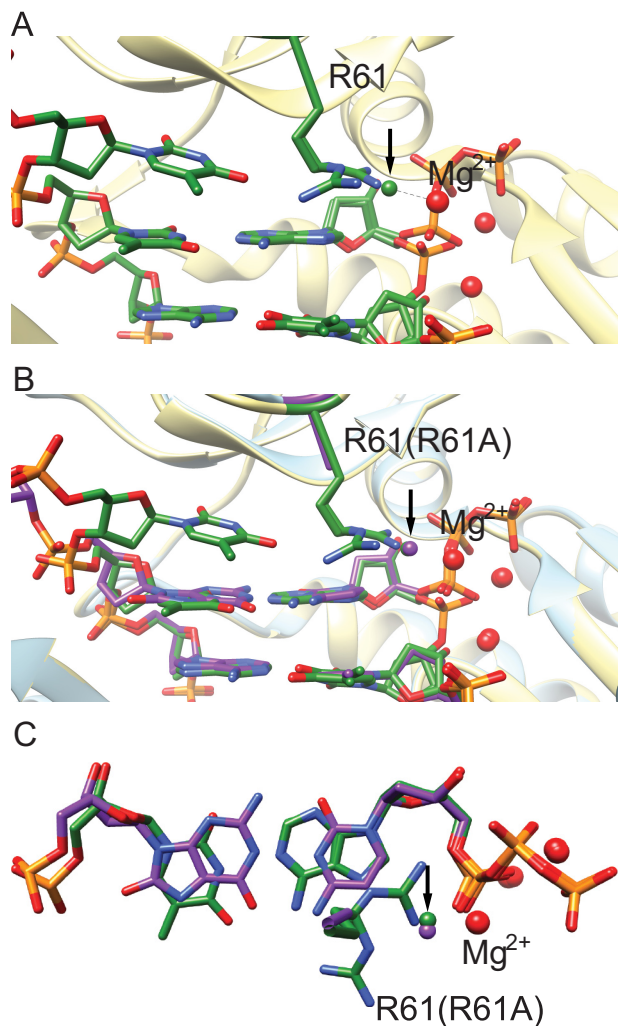


FIGURE 10. Comparison of wild-type hpol  $\eta$  during the catalytic process with Q38A/R61A-8-oxoG-dCTP. A, the ternary structure of wild-type hpol  $\eta$  during catalytic process (PDB code 4ECT (34)); B and C, active site views of superimposed structures of wild-type hpol  $\eta$  complex and Q38A/R61A-8-oxoG-dCTP from the major groove and on top of the base pair.

structure. After refinement using the program Phenix, the occupancy of  $\text{Na}^+$  was 0.38, and the  $B$  factor dropped from 35.6 to 21  $\text{Å}^2$  compared with a fully occupied water (data not presented). Thus, we cannot completely exclude the possibility that the electron density peak represents a partially occupied  $\text{Na}^+$  instead of  $\text{H}_2\text{O}$  on top of the base ring. Soaking crystals with  $\text{K}^+$  or  $\text{Rb}^+$  and collecting anomalous data may help to further resolve the issue, although  $\text{K}^+$  and  $\text{Rb}^+$  have larger ionic radii than  $\text{Na}^+$  (53).

On the other hand, the electrostatic interaction with the incoming dNTP was lost when Arg-61 was mutated to the hydrophobic Met. In addition, the side chain of R61M was too big to allow room for Arg-61-mimicking water molecules, as seen in the ternary structures with the mutation R61A. As a result, hpol  $\eta$  with the single substitution R61A was more active than with R61M. Similar results were observed with the Q38A and Q38L mutants (Tables 1 and 2 and Figs. 6 and 7).

A second unexpected result was observed from the pre-steady-state kinetic data; the burst amplitudes for wild type hpol  $\eta$  inserting dCTP opposite unmodified G or 8-oxG were

$\sim 100$  or 70% of the input, respectively, whereas the amplitude was  $< 21\%$  for either the R61M or Q38A/R61A mutant. The result indicated the presence of either an inactive form(s) of mutant protein or an equilibrium of reactive and nonreactive ternary complexes (1). Interestingly, gel filtration chromatography showed the presence of both multimeric and monomeric forms of wild type or mutants of hpol  $\eta$ . Both forms of the proteins were active and formed single crystals (data not shown; however, the extent of the multimeric state is not known at the high concentration used for crystal formation). These results suggest that hpol  $\eta$  may assemble to multimers *in vivo*, and the two mutants showed an increased tendency to multimeric assembly compared with wild-type hpol  $\eta$  (Fig. 9), although extensive cellular studies would be needed for further conclusions about physiological relevance. The reason for this change in behavior is unknown, considering that the mutations are in the interior of the protein. Interestingly, multimeric forms of the other polymerases have been reported previously. For example, *S. solfataricus* Dpo4 can form a dimer on DNA *in vitro* (54). Small angle x-ray scattering and ultracentrifugation results reveal that mammalian DNA polymerase  $\beta$  binds with DNA in ratios of both 2:1 and 1:1 in solution (55, 56). Recently, an A-family DNA polymerase (polymerase  $\theta$ ) has been reported to be able to form a dimer, which may be important for polymerase  $\theta$  to participate in microhomology-mediated end joining (57). Considering those examples, it is possible that the multimeric form(s) of hpol  $\eta$  plays a specific role in certain biological processes, although further investigation will be required.

hpol  $\eta$  has been shown to have active site prealignment, dNTP-metal ion binding, and third metal ion binding steps during its catalytic cycle (34, 38). In our study, the biochemical and structural results provide direct evidence that the conserved active site residues Arg-61 and Gln-38 synergistically contribute to enzyme efficiency and fidelity, further delineating the catalytic mechanism of the nucleotidyl transfer reaction catalyzed by hpol  $\eta$ .

*Acknowledgments*—We thank P. S. Pallan for advice on some of the crystallography work and K. Trisler for assistance in preparation of the manuscript. Vanderbilt University is a member institution of the Life Sciences Collaborative Access Team at Sector 21 of the Advanced Photon Source (Argonne, IL). Use of the Advanced Photon Source at Argonne National Laboratory was supported by the United States Department of Energy, Office of Science, Office of Basic Energy Sciences, under Contract DE-AC02-06CH11357.

## References

- Guengerich, F. P. (2006) Interactions of carcinogen-bound DNA with individual DNA polymerases. *Chem. Rev.* **106**, 420–452
- Ohmori, H., Friedberg, E. C., Fuchs, R. P. P., Goodman, M. F., Hanaoka, F., Hinkle, D., Kunkel, T. A., Lawrence, C. W., Livneh, Z., Nohmi, T., Prakash, L., Prakash, S., Todo, T., Walker, G. C., Wang, Z., and Woodgate, R. (2001) The Y-family of DNA polymerases. *Mol. Cell* **8**, 7–8
- Yang, W., and Woodgate, R. (2007) What a difference a decade makes: insights into translesion DNA synthesis. *Proc. Natl. Acad. Sci. U.S.A.* **104**, 15591–15598
- Sale, J. E., Lehmann, A. R., and Woodgate, R. (2012) Y-family DNA polymerases and their role in tolerance of cellular DNA damage. *Nat. Rev. Mol.*

- Cell Biol.* **13**, 141–152
5. Yang, W. (2014) An overview of Y-family DNA polymerases and a case study of human DNA polymerase  $\eta$ . *Biochemistry* **53**, 2793–2803
  6. Reha-Krantz, L. J. (2010) DNA polymerase proofreading: multiple roles maintain genome stability. *Biochim. Biophys. Acta* **1804**, 1049–1063
  7. Inui, H., Oh, K. S., Nadem, C., Ueda, T., Khan, S. G., Metin, A., Gozukara, E., Emmert, S., Slor, H., Busch, D. B., Baker, C. C., DiGiovanna, J. J., Tamura, D., Seitz, C. S., Gratchev, A., Wu, W. H., Chung, K. Y., Chung, H. J., Azizi, E., Woodgate, R., Schneider, T. D., and Kraemer, K. H. (2008) Xeroderma pigmentosum-variant patients from America, Europe, and Asia. *J. Invest. Dermatol.* **128**, 2055–2068
  8. Masutani, C., Kusumoto, R., Yamada, A., Dohmae, N., Yokoi, M., Yuasa, M., Araki, M., Iwai, S., Takio, K., and Hanaoka, F. (1999) The XPV (xeroderma pigmentosum variant) gene encodes human DNA polymerase  $\eta$ . *Nature* **399**, 700–704
  9. Johnson, R. E., Kondratyck, C. M., Prakash, S., and Prakash, L. (1999) hRAD30 mutations in the variant form of xeroderma pigmentosum. *Science* **285**, 263–265
  10. Zhao, Y., Biertümpfel, C., Gregory, M. T., Hua, Y. J., Hanaoka, F., and Yang, W. (2012) Structural basis of human DNA polymerase  $\eta$ -mediated chemoresistance to cisplatin. *Proc. Natl. Acad. Sci. U.S.A.* **109**, 7269–7274
  11. Gregory, M. T., Park, G. Y., Johnstone, T. C., Lee, Y. S., Yang, W., and Lippard, S. J. (2014) Structural and mechanistic studies of polymerase  $\eta$  bypass of phenanthriplatin DNA damage. *Proc. Natl. Acad. Sci. U.S.A.* **111**, 9133–9138
  12. Vaisman, A., Masutani, C., Hanaoka, F., and Chaney, S. G. (2000) Efficient translesion replication past oxaliplatin and cisplatin GpG adducts by human DNA polymerase  $\eta$ . *Biochemistry* **39**, 4575–4580
  13. Masutani, C., Kusumoto, R., Iwai, S., and Hanaoka, F. (2000) Mechanisms of accurate translesion synthesis by human DNA polymerase  $\eta$ . *EMBO J.* **19**, 3100–3109
  14. Bassett, E., King, N. M., Bryant, M. F., Hector, S., Pendyala, L., Chaney, S. G., and Cordeiro-Stone, M. (2004) The role of DNA polymerase  $\eta$  in translesion synthesis past platinum-DNA adducts in human fibroblasts. *Cancer Res.* **64**, 6469–6475
  15. Albertella, M. R., Green, C. M., Lehmann, A. R., and O'Connor, M. J. (2005) A role for polymerase  $\eta$  in the cellular tolerance to cisplatin-induced damage. *Cancer Res.* **65**, 9799–9806
  16. Chen, Y. W., Cleaver, J. E., Hanaoka, F., Chang, C. F., and Chou, K. M. (2006) A novel role of DNA polymerase  $\eta$  in modulating cellular sensitivity to chemotherapeutic agents. *Mol. Cancer Res.* **4**, 257–265
  17. Hicks, J. K., Chute, C. L., Paulsen, M. T., Ragland, R. L., Howlett, N. G., Guéranger, Q., Glover, T. W., and Canman, C. E. (2010) Differential roles for DNA polymerases eta, zeta, and REV1 in lesion bypass of intrastrand versus interstrand DNA cross-links. *Mol. Cell Biol.* **30**, 1217–1230
  18. Kawamoto, T., Araki, K., Sonoda, E., Yamashita, Y. M., Harada, K., Kikuchi, K., Masutani, C., Hanaoka, F., Nozaki, K., Hashimoto, N., and Takeda, S. (2005) Dual roles for DNA polymerase  $\eta$  in homologous DNA recombination and translesion DNA synthesis. *Mol. Cell* **20**, 793–799
  19. McIlwraith, M. J., Vaisman, A., Liu, Y., Fanning, E., Woodgate, R., and West, S. C. (2005) Human DNA polymerase  $\eta$  promotes DNA synthesis from strand invasion intermediates of homologous recombination. *Mol. Cell* **20**, 783–792
  20. Bugreev, D. V., Hanaoka, F., and Mazin, A. V. (2007) Rad54 dissociates homologous recombination intermediates by branch migration. *Nat. Struct. Mol. Biol.* **14**, 746–753
  21. Zhao, Y., Gregory, M. T., Biertümpfel, C., Hua, Y. J., Hanaoka, F., and Yang, W. (2013) Mechanism of somatic hypermutation at the WA motif by human DNA polymerase  $\eta$ . *Proc. Natl. Acad. Sci. U.S.A.* **110**, 8146–8151
  22. Zeng, X., Winter, D. B., Kasper, C., Kraemer, K. H., Lehmann, A. R., and Gearhart, P. J. (2001) DNA polymerase  $\eta$  is an A-T mutator in somatic hypermutation of immunoglobulin variable genes. *Nat. Immunol.* **2**, 537–541
  23. Delbos, F., De Smet, A., Faili, A., Aoufouchi, S., Weill, J. C., and Reynaud, C. A. (2005) Contribution of DNA polymerase  $\eta$  to immunoglobulin gene hypermutation in the mouse. *J. Exp. Med.* **201**, 1191–1196
  24. Pavlov, Y. I., Rogozin, I. B., Galkin, A. P., Aksenova, A. Y., Hanaoka, F., Rada, C., and Kunkel, T. A. (2002) Correlation of somatic hypermutation specificity and A-T base pair substitution errors by DNA polymerase  $\eta$  during copying of a mouse immunoglobulin kappa light chain transgene. *Proc. Natl. Acad. Sci. U.S.A.* **99**, 9954–9959
  25. Rogozin, I. B., and Pavlov, Y. I. (2003) Theoretical analysis of mutation hotspots and their DNA sequence context specificity. *Mutat. Res.* **544**, 65–85
  26. Wilson, T. M., Vaisman, A., Martomo, S. A., Sullivan, P., Lan, L., Hanaoka, F., Yasui, A., Woodgate, R., and Gearhart, P. J. (2005) MSH2-MSH6 stimulates DNA polymerase  $\eta$ , suggesting a role for A:T mutations in antibody genes. *J. Exp. Med.* **201**, 637–645
  27. Delbos, F., Aoufouchi, S., Faili, A., Weill, J. C., and Reynaud, C. A. (2007) DNA polymerase  $\eta$  is the sole contributor of A/T modifications during immunoglobulin gene hypermutation in the mouse. *J. Exp. Med.* **204**, 17–23
  28. Silverstein, T. D., Jain, R., Johnson, R. E., Prakash, L., Prakash, S., and Aggarwal, A. K. (2010) Structural basis for error-free replication of oxidatively damaged DNA by yeast DNA polymerase  $\eta$ . *Structure* **18**, 1463–1470
  29. Haracska, L., Yu, S. L., Johnson, R. E., Prakash, L., and Prakash, S. (2000) Efficient and accurate replication in the presence of 7,8-dihydro-8-oxoguanine by DNA polymerase  $\eta$ . *Nat. Genet.* **25**, 458–461
  30. Patra, A., Nagy, L. D., Zhang, Q., Su, Y., Müller, L., Guengerich, F. P., and Egli, M. (2014) Kinetics, structure, and mechanism of 8-oxo-7,8-dihydro-2'-deoxyguanosine bypass by human DNA polymerase  $\eta$ . *J. Biol. Chem.* **289**, 16867–16882
  31. van Loon, B., Markkanen, E., and Hübscher, U. (2010) Oxygen as a friend and enemy: how to combat the mutational potential of 8-oxo-guanine. *DNA Repair* **9**, 604–616
  32. Maga, G., Villani, G., Crespan, E., Wimmer, U., Ferrari, E., Bertocci, B., and Hübscher, U. (2007) 8-Oxo-guanine bypass by human DNA polymerases in the presence of auxiliary proteins. *Nature* **447**, 606–608
  33. Zahn, K. E., Wallace, S. S., and Doublé, S. (2011) DNA polymerases provide a canon of strategies for translesion synthesis past oxidatively generated lesions. *Curr. Opin. Struct. Biol.* **21**, 358–369
  34. Nakamura, T., Zhao, Y., Yamagata, Y., Hua, Y. J., and Yang, W. (2012) Watching DNA polymerase  $\eta$  make a phosphodiester bond. *Nature* **487**, 196–201
  35. Biertümpfel, C., Zhao, Y., Kondo, Y., Ramón-Maiques, S., Gregory, M., Lee, J. Y., Masutani, C., Lehmann, A. R., Hanaoka, F., and Yang, W. (2010) Structure and mechanism of human DNA polymerase  $\eta$ . *Nature* **465**, 1044–1048
  36. Silverstein, T. D., Johnson, R. E., Jain, R., Prakash, L., Prakash, S., and Aggarwal, A. K. (2010) Structural basis for the suppression of skin cancers by DNA polymerase  $\eta$ . *Nature* **465**, 1039–1043
  37. Patra, A., Zhang, Q., Lei, L., Su, Y., Egli, M., and Guengerich, F. P. (2015) Structural and kinetic analysis of nucleoside triphosphate incorporation opposite an abasic site by human translesion DNA polymerase  $\eta$ . *J. Biol. Chem.* **290**, 8028–8038
  38. Ummat, A., Silverstein, T. D., Jain, R., Buku, A., Johnson, R. E., Prakash, L., Prakash, S., and Aggarwal, A. K. (2012) Human DNA polymerase  $\eta$  is pre-aligned for dNTP binding and catalysis. *J. Mol. Biol.* **415**, 627–634
  39. Schorr, S., Schneider, S., Lammens, K., Hopfner, K. P., and Carell, T. (2010) Mechanism of replication blocking and bypass of Y-family polymerase  $\eta$  by bulky acetylaminofluorene DNA adducts. *Proc. Natl. Acad. Sci. U.S.A.* **107**, 20720–20725
  40. Sassa, A., Beard, W. A., Shock, D. D., and Wilson, S. H. (2013) Steady-state, pre-steady-state, and single-turnover kinetic measurement for DNA glycosylase activity. *J. Vis. Exp.* 10.3791/50695
  41. Otwinowski, Z., and Minor, W. (1997) Processing of x-ray diffraction data collected in oscillation mode. *Methods Enzymol.* **276**, 307–326
  42. McCoy, A. J., Grosse-Kunstleve, R. W., Adams, P. D., Winn, M. D., Storoni, L. C., and Read, R. J. (2007) Phaser crystallographic software. *J. Appl. Crystallogr.* **40**, 658–674
  43. Adams, P. D., Afonine, P. V., Bunkóczi, G., Chen, V. B., Davis, I. W., Echols, N., Headd, J. J., Hung, L. W., Kapral, G. J., Grosse-Kunstleve, R. W., McCoy, A. J., Moriarty, N. W., Oeffner, R., Read, R. J., Richardson, D. C., Richardson, J. S., Terwilliger, T. C., and Zwart, P. H. (2010) PHENIX: a

- comprehensive Python-based system for macromolecular structure solution. *Acta Crystallogr. D Biol. Crystallogr.* **66**, 213–221
44. Langer, G. G., Hazledine, S., Wiegels, T., Carolan, C., and Lamzin, V. S. (2013) Visual automated macromolecular model building. *Acta Crystallogr. D Biol. Crystallogr.* **69**, 635–641
  45. Murshudov, G. N., Skubák, P., Lebedev, A. A., Pannu, N. S., Steiner, R. A., Nicholls, R. A., Winn, M. D., Long, F., and Vagin, A. A. (2011) REFMAC5 for the refinement of macromolecular crystal structures. *Acta Crystallogr. D Biol. Crystallogr.* **67**, 355–367
  46. Emsley, P., Lohkamp, B., Scott, W. G., and Cowtan, K. (2010) Features and development of Coot. *Acta Crystallogr. D Biol. Crystallogr.* **66**, 486–501
  47. Pettersen, E. F., Goddard, T. D., Huang, C. C., Couch, G. S., Greenblatt, D. M., Meng, E. C., and Ferrin, T. E. (2004) UCSF Chimera: a visualization system for exploratory research and analysis. *J. Comput. Chem.* **25**, 1605–1612
  48. Furge, L. L., and Guengerich, F. P. (1999) Explanation of pre-steady-state kinetics and decreased burst amplitude of HIV-1 reverse transcriptase at sites of modified DNA bases with an additional, nonproductive enzyme-DNA-nucleotide complex. *Biochemistry* **38**, 4818–4825
  49. Egli, M., and Sarkhel, S. (2007) Lone pair-aromatic interactions: to stabilize or not to stabilize. *Acc. Chem. Res.* **40**, 197–205
  50. Eoff, R. L., Irimia, A., Angel, K. C., Egli, M., and Guengerich, F. P. (2007) Hydrogen bonding of 7,8-dihydro-8-oxodeoxyguanosine with a charged residue in the little finger domain determines miscoding events in *Sulfolobus solfataricus* DNA polymerase Dpo4. *J. Biol. Chem.* **282**, 19831–19843
  51. Suarez, S. C., Beardslee, R. A., Toffton, S. M., and McCulloch, S. D. (2013) Biochemical analysis of active site mutations of human polymerase  $\eta$ . *Mutat. Res.* **745**, 46–54
  52. Wouters, J. (1998) Cation- $\pi$  ( $\text{Na}^+$ -Trp) interactions in the crystal structure of tetragonal lysozyme. *Protein Sci.* **7**, 2472–2475
  53. Tereshko, V., Wilds, C. J., Minasov, G., Prakash, T. P., Maier, M. A., Howard, A., Wawrzak, Z., Manoharan, M., and Egli, M. (2001) Detection of alkali metal ions in DNA crystals using state-of-the-art x-ray diffraction experiments. *Nucleic Acids Res.* **29**, 1208–1215
  54. Lin, H. K., Chase, S. F., Laue, T. M., Jen-Jacobson, L., and Trakselis, M. A. (2012) Differential temperature-dependent multimeric assemblies of replication and repair polymerases on DNA increase processivity. *Biochemistry* **51**, 7367–7382
  55. Tang, K. H., Niebuhr, M., Aulabaugh, A., and Tsai, M. D. (2008) Solution structures of 2:1 and 1:1 DNA polymerase-DNA complexes probed by ultracentrifugation and small-angle x-ray scattering. *Nucleic Acids Res.* **36**, 849–860
  56. Tang, K. H., and Tsai, M. D. (2008) Structure and function of 2:1 DNA polymerase-DNA complexes. *J. Cell Physiol.* **216**, 315–320
  57. Kent, T., Chandramouly, G., McDevitt, S. M., Ozdemir, A. Y., and Pomerantz, R. T. (2015) Mechanism of microhomology-mediated end-joining promoted by human DNA polymerase  $\theta$ . *Nat. Struct. Mol. Biol.* **22**, 230–237

**DNA and Chromosomes:**  
**Roles of Residues Arg-61 and Gln-38 of**  
**Human DNA Polymerase  $\eta$  in Bypass of**  
**Deoxyguanosine and 7,8-Dihydro-8-oxo-2'**  
**-deoxyguanosine**



Yan Su, Amritraj Patra, Joel M. Harp, Martin  
Egli and F. Peter Guengerich  
*J. Biol. Chem.* 2015, 290:15921-15933.  
doi: 10.1074/jbc.M115.653691 originally published online May 6, 2015

Access the most updated version of this article at doi: [10.1074/jbc.M115.653691](https://doi.org/10.1074/jbc.M115.653691)

Find articles, minireviews, Reflections and Classics on similar topics on the [JBC Affinity Sites](#).

Alerts:

- [When this article is cited](#)
- [When a correction for this article is posted](#)

[Click here](#) to choose from all of JBC's e-mail alerts

This article cites 57 references, 20 of which can be accessed free at  
<http://www.jbc.org/content/290/26/15921.full.html#ref-list-1>